Chemistry & Biology
Article

Biomembrane Interactions Reveal the Mechanism of Action of Surface-Immobilized Host Defense IDR-1010 Peptide

Guangzheng Gao,[1,2,5] John T.J. Cheng,[3,5] Jason Kindrachuk,[4] Robert E.W. Hancock,[4] Suzana K. Straus,[3,*] and Jayachandran N. Kizhakkedathu[1,2,3,*]
[1]Centre for Blood Research
[2]Department of Pathology and Laboratory Medicine
University of British Columbia, 2350 Health Sciences Mall, Vancouver, British Columbia V6T 1Z3, Canada
[3]Department of Chemistry, University of British Columbia, Vancouver, British Columbia V6T 1Z1, Canada
[4]Centre for Microbial Diseases and Immunity Research, University of British Columbia, 2259 Lower Mall Research Station, Vancouver, British Columbia V6T 1Z3, Canada
[5]These authors contributed equally to this work
*Correspondence: sstraus@chem.ubc.ca (S.K.S.), jay@pathology.ubc.ca (J.N.K.)
DOI 10.1016/j.chembiol.2011.12.015

SUMMARY

Dissecting the mechanism of action of surface-tethered antimicrobial and immunomodulatory peptides is critical to the design of optimized anti-infection coatings on biomedical devices. To address this, we compared the biomembrane interactions of host defense peptide IDR-1010cys (1) in free form, (2) as a soluble polymer conjugate, and (3) with one end tethered to a solid support with model bacterial and mammalian lipid membranes. Our results show that IDR-1010cys in all three distinct forms interacted with bacterial and mammalian lipid vesicles, but the extent of the interactions as monitored by the induction of secondary structure varied. The enhanced interaction of surface-tethered peptides is well correlated with their very good antimicrobial activities. Our results demonstrate that there may be a difference in the mechanism of action of surface-tethered versus free IDR-1010cys.

INTRODUCTION

The availability of biocompatible anti-infective surfaces with broad-spectrum antimicrobial activity would significantly decrease the infection rates associated with biomedical devices and implants. Two to six percent of inserted implants (cardiovascular, orthopedic, neurosurgical, plastic surgical, and urologic) are associated with infection (Costerton et al., 1999; Darouiche, 2001, 2004; Foxman, 2002; Trampuz and Widmer, 2006; Zimmerli et al., 2004). Although this may not seem problematic, the associated average cost of combined medical and surgical treatments is several thousand dollars per patient in these cases and represents a significant economic burden on the health care system (Foxman, 2002; Trampuz and Widmer, 2006; Zimmerli et al., 2004). Several approaches have been reported for the development of infection-resistant surfaces using both covalent and noncovalent methods for attaching antimicrobial agents onto the surface (Blin et al., 2011; Gao et al., 2011a; Glinel et al., 2009; Hetrick and Schoenfisch, 2006; Matl et al., 2008; Noimark et al., 2009; Ramstedt et al., 2009; Sambhy et al., 2006; Shukla et al., 2010; Gollwitzer et al., 2003; Palermo et al., 2011). Some of these methods showed very promising antimicrobial and antibiofilm properties with excellent biocompatibility (Gao et al., 2011a; Glinel et al., 2009; Shukla et al., 2010).

Host defense peptides (HDPs) are integral components of the immune defenses of nearly every living organism and play a central role in the innate immune system of plants, insects, and higher vertebrates (Bowdish et al., 2005; Mookherjee et al., 2006; Scott et al., 2007). These short peptides are typically amphipathic and possess an overall net positive charge, arising from the presence of large numbers of lysine and arginine residues. Typically, HDPs are unstructured in solution and adopt a defined conformation in the presence of phospholipids or in a hydrophobic environment (Straus and Hancock, 2006). This change in conformation upon binding to the membrane is widely viewed as the first step of a peptide's mechanism of action. Folded peptides fall into four broad structural groups: β sheet, α helix, loop, and extended structures. HDPs kill microbes through modulation of the immune system. When HDPs directly kill microbes under physiological conditions, they are then also termed antimicrobial peptides (AMPs) (Gottler and Ramamoorthy, 2009).

We have recently demonstrated that surface-tethered AMPs preserve their broad-spectrum antimicrobial activity against bacteria (Gao et al., 2011a, 2011b). However, there is currently limited knowledge of the detailed mechanism of action of surface-tethered AMPs (Bagheri et al., 2009; Onaizi and Leong, 2011). For instance, it is unknown whether surface-tethered AMPs adopt defined structures when they interact with membranes. Moreover, it is unclear whether tethered peptides perturb membrane bilayers in a similar manner as their free peptide counterparts.

To address this paucity of mechanistic data, we have investigated the biomembrane interactions of the short-chain antimicrobial and immunomodulatory peptide innate defense regulator (IDR) 1010 in its free form (referred throughout the

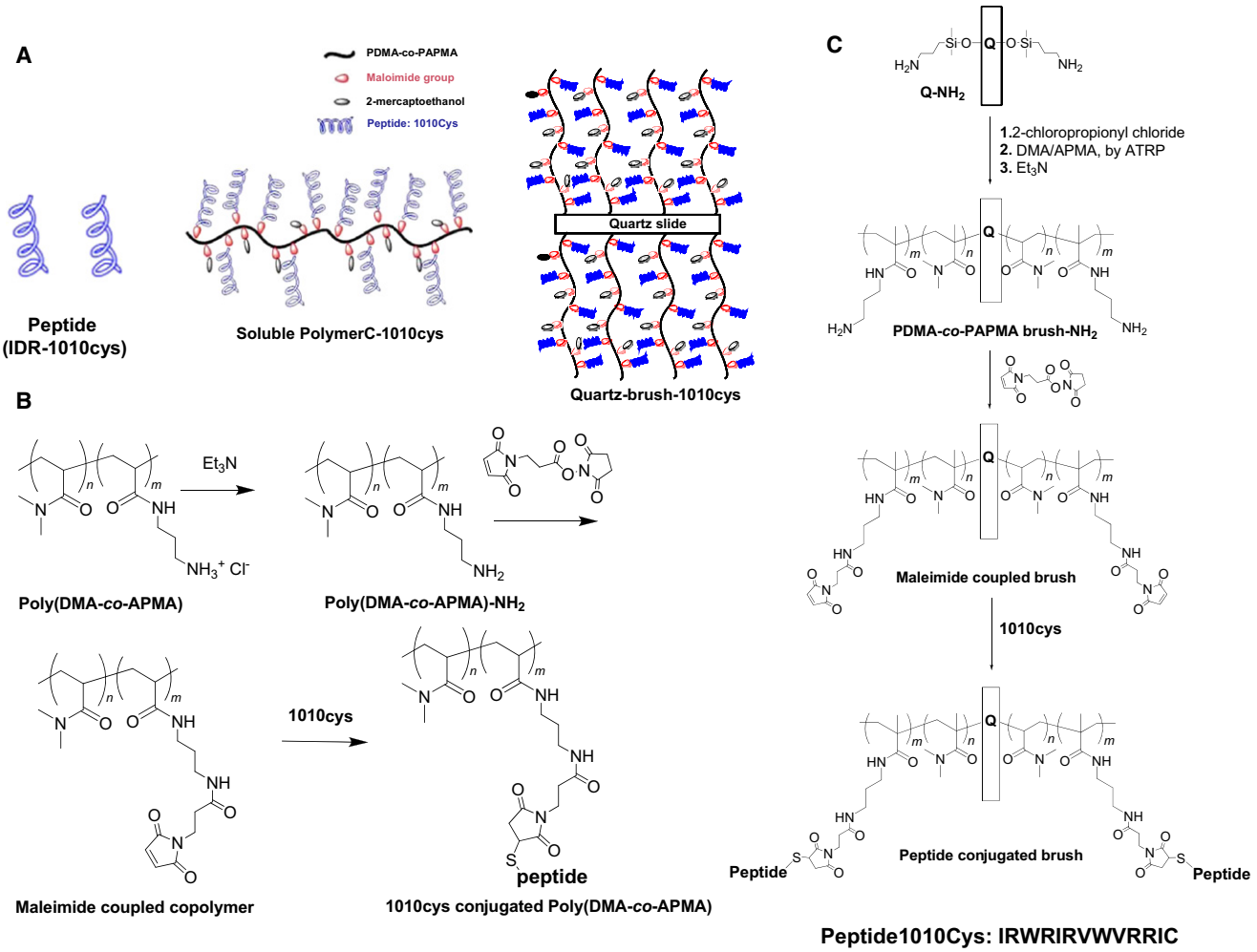

Figure 1. Schematic Representation of Peptide Forms and Their Synthesis

(A) Idealized representation of peptide IDR-1010cys in different forms used in this study.

(B) Synthesis of IDR-1010cys-conjugated soluble poly(DMA-*co*-APMA) copolymer (polymerC-1010cys).

(C) Synthetic scheme for polymer brush-tethered IDR-1010cys on a quartz surface (quartz-brush-1010cys).

paper as "1010cys"), as a soluble polymer conjugate ("polymerC-1010cys"), and in surface-tethered form ("quartz-brush-1010cys"), which is achieved through single end attachment of the peptide to a hydrophilic polymer brush (Figure 1A). We investigated the conformation of the peptide in these three different forms in the presence of model bacterial and mammalian lipids using circular dichroism (CD). This study provides unique insight into the mechanism of action of surface-immobilized host defense peptides.

RESULTS

Selection of IDR-1010

Peptide IDR-1010 (IRWRIRVWVRRI-NH_2) was selected from a library of peptides that includes IDRs 1002, 1018, and HH2 (Wieczorek et al., 2010; Nijnik et al., 2010; Kindrachuk et al., 2009). This peptide library was generated by the substituting and scrambling of amino acids, using the bovine peptide bactenecin as a basic template. IDR-1010 demonstrated good antimicrobial activity against *Staphylococcus aureus* (minimal inhibitory concentration [MIC] = 2.3 μg/ml) and *Pseudomonas aeruginosa* (MIC = 9 μg/ml). In addition, it demonstrated minimal toxicity toward mammalian cells, demonstrating only 22% lysis of human red blood cells at 375 μg/ml (data not shown). It was also one of the most exceptional immunomodulatory peptides, with an ability to induce 706 pg/ml of chemokine monocyte chemoattractant protein 1 (MCP-1) at a peptide concentration of 20 μg/ml and 5,662 pg/ml of MCP-1 at 100 μg/ml. It also demonstrated a potent ability to suppress endotoxin lipopolysaccharide (LPS)-mediated induction of the pro-inflammatory cytokine TNF-α in human peripheral blood mononuclear cells (PBMCs) by 94%. It also completely protected mice against an invasive *S. aureus* infection when given intraperitoneally to mice at 8 mg/kg 4 hr prior to initiation of the infection (data not shown). In these regards, its activity was consistent with those of previously described IDR peptides 1002 and 1018.

Table 1. Characteristics of IDR-1010cys-Conjugated Poly(DMA-*co*-APMA) Brush on Quartz Surface; Quartz-Brush-1010cys

Sample[a]	[DMA]/[APMA][b]	M_n[c] ($\times 10^{-4}$)	M_w/M_n[c]	Dry Brush Thickness[d] Before Conjugation *h* (nm)	Dry Brush Thickness[d] After Conjugation *h* (nm)	Graft Density[e] (Chains/nm^2)	Peptides/Chain	Peptides/nm^2	Mass of Peptides (μg/cm^2)	Concentration on the Surface (mol/l)
Q-1-1	1.0/1	16.67	1.18	33.8 ± 0.8	72.7 ± 0.9	0.15	50	7.5	2.52	0.17
Q-3-1	3.0/1	15.63	1.54	34.7 ± 0.7	82.6 ± 2.5	0.16	98	15.68	5.27	0.31
Q-5-1	4.8/1	16.09	1.68	37.8 ± 0.9	84.7 ± 4.4	0.16	100	16.0	5.38	0.31

[a] ATRP conditions: $[HMTETA]_0/[CuCl]_0/[CuCl_2]_0/[I]_0/([DMA]_0 + [APMA]_0) = 2.2/1/0.1/0.1/156$, $[DMA]_0 + [APMA]_0 = 1.2$ mol/l, 22°C, 24 hr. Peptide: IDR-1010cys.
[b] Determined by ^{1}H NMR of soluble polymers (Figure S2).
[c] Determined by gel permeation chromatography.
[d] Determined by AFM scratch analysis.; standard deviations are based on thickness measurements at five different locations on the sample.
[e] Calculated by Equation 1. Concentration on the surface (mol/l) was calculated from the dry thickness of the brush after peptide conjugation and the mass of the peptides/cm^2 (see Figure S1 and Supplemental Experimental Procedures).

Following the soluble polymer conjugation of IDR-1010cys (see also below), the MIC for *P. aeruginosa* increased by only 4-fold whereas the immunomodulatory activity was substantially reduced but still evident, with 463 pg/ml of MCP-1 induced at 100 μg/ml (Table S1 available online).

Synthesis of Peptide-Conjugated Copolymer Brushes

Three types of primary amine-containing copolymer brushes were synthesized on quartz surfaces, and their characteristics are given in Table 1. The molecular weight and composition of the grafted chains on the quartz surface were taken as equal to that of soluble polymer chains formed along with the grafted chains, as this is common practice for the characterization of polymer brushes on flat surfaces (Zou et al., 2009; Barbey et al., 2009; Husseman et al., 1999; Iwata et al., 2008; Kizhakkedathu and Brooks, 2003). This is due to the very small amount of polymer that can be cleaved from the surface for characterization.

Figure 1C details the synthetic steps involved in tethering one end of IDR-1010cys to copolymer brushes via a maleimide-thiol addition reaction. The characteristic absorption at $\lambda = 280$ nm in the UV-vis spectra (Figure 2A) of peptide-conjugated quartz slides demonstrated the peptide conjugation. The formation of the poly(*N*,*N*-dimethylacrylamide-*co*-(3-aminopropyl)methacrylamide hydrochloride) (poly(DMA-*co*-APMA)) brush and the immobilization of IDR-1010cys were evident from the characteristic peaks for the polymer and peptide in the attenuated total reflectance-Fourier transform infrared spectroscopy (ATR-FTIR) spectra (Figure 2B). Further evidence for copolymer brush formation and peptide conjugation was obtained from the dry thickness measurements by atomic force microscopy (AFM) obtained after scratching the surface. A considerable increase in the thickness of the copolymer brush was observed after peptide conjugation (Table 1). Because there were no new grafted polymer chains added to the surface in the peptide conjugation step, the increase in layer thickness was attributed to the increase in molecular weight following peptide coupling (Figure S1). Thus, from the increase in dry thickness of the polymer-grafted layer, the number of peptides/chains and the peptide density (Table 1) on the surface were calculated (see Supplemental Information for details) (Gao et al., 2011a, 2011b).

Synthesis of Soluble Copolymer Conjugated to Peptide IDR-1010cys

Figure 1B shows the scheme for the coupling of peptides to soluble poly(DMA-*co*-APMA) (polymerC-1010cys). The soluble copolymer formed during the surface grafting at the composition ratio DMA:APMA (1:1) was used. The M_n of the copolymer was 166, 700 with a polydispersity of 1.18. The experimentally determined composition of the copolymer was close to 1:1 DMA:APMA (for ^{1}H NMR spectra, see Figure S2). The maleimide groups were introduced before the IDR-1010cys conjugation via a Michael-type addition (Figure 1B). The presence of characteristic peaks of peptide in the FTIR spectrum of conjugate (Figure 2C) confirms its formation. The disappearance of the maleimide peak at 6.77 ppm in the ^{1}H NMR spectrum of polymerC-1010cys also supported this (Figure S3). UV-vis analysis showed that ~300 peptides grafted per polymer chain. The IDR-1010cys-conjugated copolymer was initially soluble in water, but following refrigerated storage at 4°C for multiple weeks the peptide conjugate was difficult to solubilize in aqueous media.

Structural Studies of Soluble Systems: IDR-1010cys and Copolymer-Conjugated IDR-1010cys; PolymerC-1010cys

Figure 3 shows the solution CD results of IDR-1010cys and polymerC-1010cys in H_2O, PBS, dodecylphosphocholine (DPC) small unilamellar vesicles (SUVs), and 1:1 dimyristoylphosphatidylcholine:dimyristoylphosphatidylglycerol (DMPC:DMPG) (mol/mol) SUVs. DPC and DMPC/DMPG lipid membranes are used as models for mammalian cell membranes and bacterial cell membranes, respectively. In H_2O and PBS, both spectra consisted of a minimum at ~200 nm, which is characteristic of random coil. In the presence of lipid SUVs, all spectra consist of a maximum at 190 nm and two minima at 207 and 222 nm, which are characteristic of α-helical structure. This demonstrated that IDR-1010cys in the free form was unstructured in an aqueous environment in the absence of lipids but adopted an α-helical conformation in the presence of lipid membranes (Figures 3A–3C). In the presence of lipid SUVs, the soluble polymerC-1010cys assumed a more structured conformation compared to that in H_2O and PBS (Figures 3D–3F). This indicated that the conjugation to polymer did not severely interfere with the peptide conformational change.

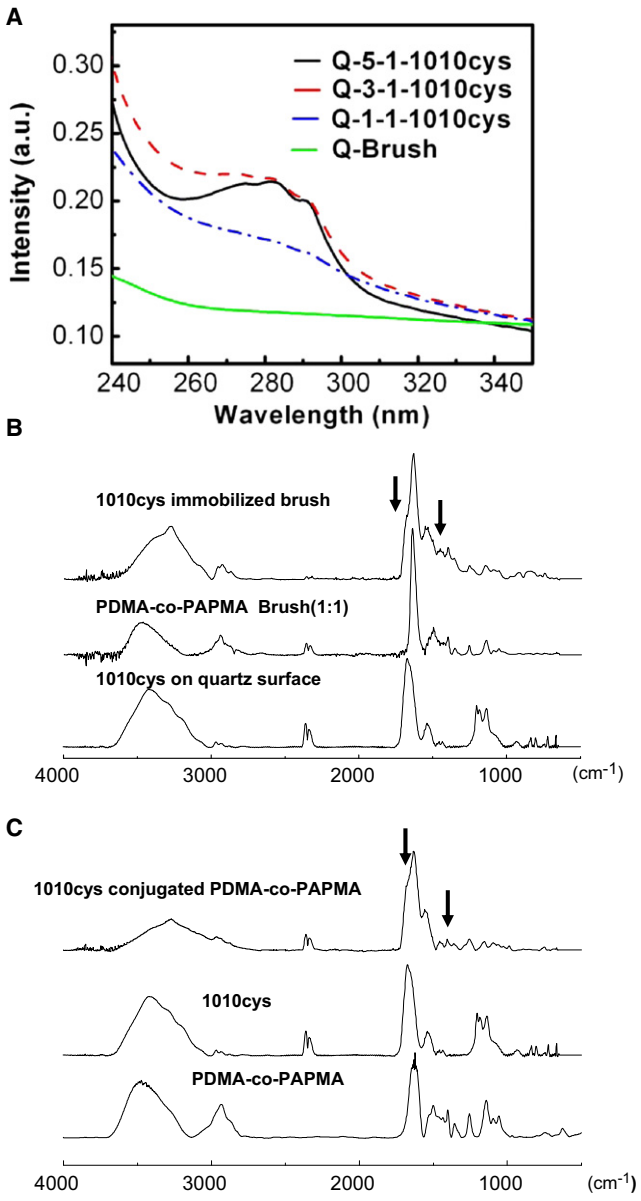

Figure 2. Characterization of Surface-Tethered IDR-1010cys and Soluble Conjugates

(A) UV-vis spectra of quartz-brush-1010cys.

(B) ATR-FTIR spectra of quartz-brush-1010cys, copolymer brush before peptide conjugation, and IDR-1010cys.

(C) FTIR spectra of soluble poly(DMA-*co*-APMA) (1:1), IDR-1010cys, and peptide-conjugated poly(DMA-*co*-APMA).

To examine the secondary structure content of IDR-1010cys and polymerC-1010cys in different environments, all spectra were fitted using three different programs (CDSSTR, CONTINLL, and SELCON3) (Cheng et al., 2010, 2011; Goux, 2002; Sreerama et al., 2000, 2001). It is important to note that the percentages of secondary structures obtained from these three programs should not be interpreted as absolute values, as the numbers vary somewhat from program to program. An average value is reported in the following and should be used in a qualitative sense.

In H_2O and PBS, IDR-1010cys in the free form showed a considerable amount of β sheet/strand (~45%) and random coil (~35%) structures. Figure 4A shows the % structural content of IDR-1010cys in the presence of DPC SUVs at different peptide-to-lipid (P:L) ratios. In the presence of DPC SUVs, IDR-1010cys adopted close to 100% α-helical conformation at all P:L ratios examined. Figure 4C shows the % structural content of soluble polymerC-1010cys in the presence of DPC at different P:L ratios. The polymer-coupled IDR-1010cys only retained ~20% α-helical structure and ~58% β sheet/strand, and the remaining was composed of random coil. The data showed that polymerC-1010cys interacted differently with DPC SUVs compared to IDR-1010cys in the free form. However, a comparison of the secondary structure content of polymerC-1010cys in DPC with that obtained in PBS in the absence of lipids showed that there was an increase in helical content. Figure 4B shows the % structural content of IDR-1010cys in the presence of DMPC/DMPG SUVs at different P:L ratios. In the presence of 1:1 DMPC:DMPG (mol/mol) SUVs, IDR-1010cys adopted ~98% α-helical conformation at high peptide concentrations and ~61% α-helical conformation at low peptide concentrations. PolymerC-1010cys retained similar % α-helical structure as in the DPC SUVs at all P:L molar ratios examined (i.e., ~20%). This indicated that the peptide conformational change did not depend significantly on the type of lipid membrane. In addition, the data from polymerC-1010cys suggested that the arrangement of IDR-1010cys on the polymer might limit its access to the lipid membrane surfaces. Consequently, only a subset of peptides could adopt the helical structure that they favored in the free form.

Structural Studies of Surface-Immobilized IDR-1010cys; Quartz-Brush-1010cys

To examine the peptide conformation in the tethered state, IDR-1010cys-immobilized copolymer brushes on quartz slides were used. Figure 5A shows CD spectra of quartz-brush-1010cys (DMA:APMA composition [1:1]) in the dry state, H_2O, PBS, and in two lipid SUVs consisting of either DPC or DMPC:DMPG (1:1). The lipid concentrations were varied from 25 to 75 mM in the case of DPC SUVs and 0.25, 0.5, and 0.75 mM for DMPC/DMPG SUVs.

In the dry state, all spectra consisted of a broad minimum at ~207 nm and a maximum at ~195 nm, which are characteristic of a mixture of α helix, β sheet/strand, and random coil. Similar spectral characteristics were observed in aqueous environment. This suggested that the peptide secondary structure was formed mainly through interactions of the grafted copolymer chains and the conjugated peptide irrespective of its surroundings. An aqueous environment in the absence of lipids did not have a significant impact on the copolymer-peptide interaction, nor did it promote peptide unfolding to give much higher random coil content.

In the presence of DPC SUVs, the spectra consisted of a broad minimum at ~207 nm, a less prominent minimum at ~222 nm, and a maximum at ~195 nm, which are characteristic of α-helical structure. This indicated that the peptide conformation changed in response to the presence of lipid membranes. In the presence of 1:1 DMPC:DMPG (mol/mol) SUVs, spectra with similar qualitative characteristics were obtained.

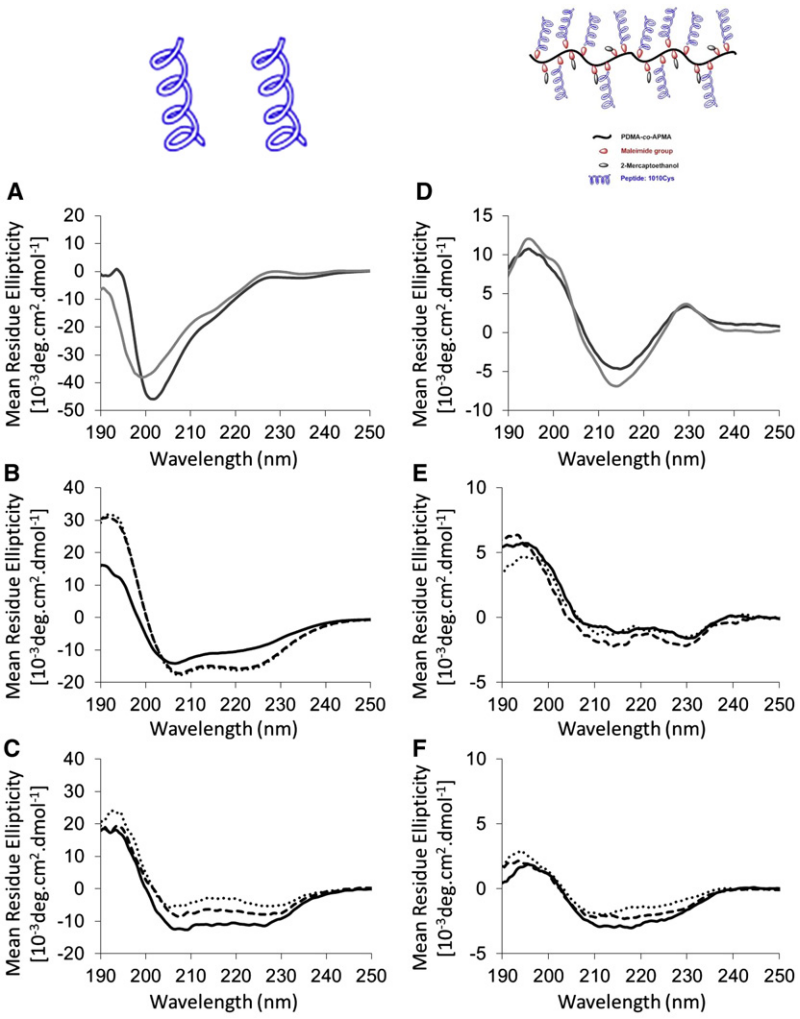

Figure 3. Biomembrane Interactions of IDR-1010cys in Free Form and Its Soluble Conjugate

Solution CD spectra of IDR-1010cys (left) and polymerC-1010cys (right) in the presence of (A) and (D) H_2O (black) and PBS (gray); (B) and (E) DPC SUVs; and (C) and (F) 1:1 DMPC:DMPG SUVs. The samples in DPC were run at peptide-to-lipid ratios of 1:15 (solid), 1:50 (dashed), and 1:100 (dotted). The samples in DMPC/DMPG were run at P:L ratios of 1:1.5 (solid), 1:5 (dashed), and 1:10 (dotted).

The structural content of quartz surface-tethered IDR-1010cys was also inspected in different environments. Figure 5B shows % α helix, % β sheet/strand, and % random coil as a function of the different lipid compositions. In the presence of DPC SUVs, the percentage of α helix increased with increasing lipid concentration. This corresponded to a decrease in random coil structure (Figure 5Ba). A sharp increase in the amount of α-helical content was observed at 25 mM DPC compared to that of PBS buffer and a gradual increase thereafter (50 and 75 mM). The percentage of structural content of quartz-brush-1010cys in the presence of DMPC:DMPG (1:1) at different lipid compositions (0.25–0.75 mM) is shown in Figure 5Bb; a gradual increase in α-helical content was seen with increasing lipid concentration. The % β sheet/strand increased initially in the presence of DMPC/DMPG but at higher concentrations of lipid it decreased. The lipid concentrations were 100-fold lower in these cases in comparison to DPC.

Similar results were obtained for quartz-brush-1010cys made with different DMA:APMA ratios. The dependence of % α helix on brush composition in different lipid membranes is shown in Figure 5Bc. There was a slight increase in the structural content of the peptides obtained as the amount of DMA in the brush was increased. These results demonstrated that even though the peptide was tethered to the polymer brush on the surface, the lipid membrane was still able to interact strongly with the peptides. Interestingly, the peptides appeared to adopt a better-defined structure when the polymer was attached to the quartz slide than when the polymer was in the soluble form for the current copolymer system. These results are well correlated with the strong antimicrobial activity of surface-tethered IDR-1010cys against *P. aeruginosa* (Figure S5) indicative of its membrane interaction. The control experiments with unmodified quartz slides and quartz slides carrying copolymer brush without peptides displayed no activity. Greater than 85% bacterial killing was observed within 4 hr, demonstrating the potent bactericidal activity of surface-immobilized IDR-1010cys.

DISCUSSION

It has been suggested that immunomodulatory and antimicrobial peptides adopt well-defined structures that directly relate to their immunomodulatory and antimicrobial functions (Wieczorek et al., 2010). These conformational changes are often observed by examining the structure of free peptides in the presence of SUVs in solution. Recent reports have shown that surface-tethered antimicrobial peptides exhibit excellent broad-spectrum antimicrobial activity and are potential candidates for the development of infection-resistant implant coatings (Bagheri et al., 2009; Onaizi and Leong, 2011; Hilpert et al., 2005, 2009; Gao et al., 2011a). Although these novel antimicrobial surfaces have intriguing activities, there is no clear understanding of how the mechanism of action of surface-immobilized peptides relates to the modes of action traditionally proposed for free peptides (Bagheri et al., 2009; Onaizi and Leong, 2011). To address this, we investigated the interactions of an immunomodulatory/antimicrobial peptide, IDR-1010, with two model lipid membranes (bacterial [DMPC/DMPG] and mammalian [DPC]) using CD spectroscopy. The conformational properties of the peptide IDR-1010cys under three entirely different experimental conditions (Figure 1A) were measured: peptide in the free form, peptide conjugated to a soluble polymer (both in solution), and surface-immobilized peptide (attached to a quartz support via a polymer brush), and the results were compared.

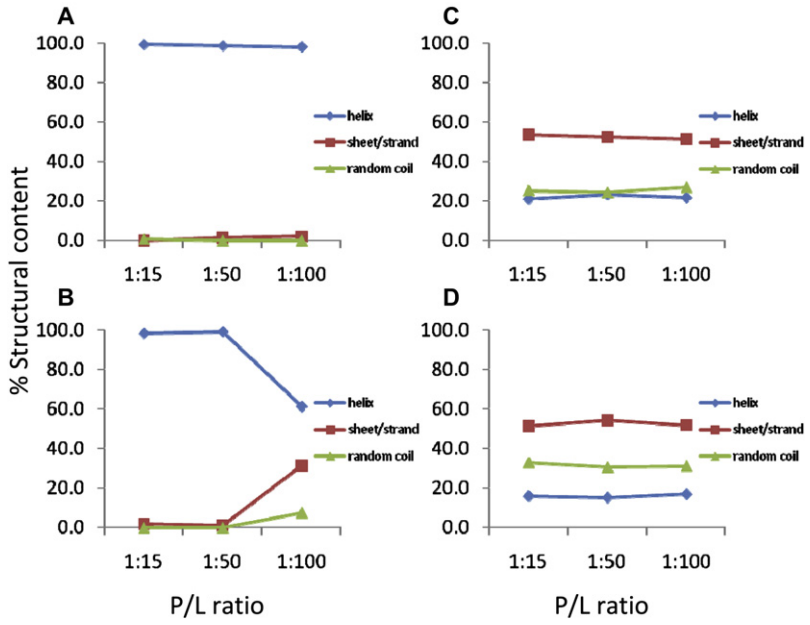

Figure 4. Secondary Structure Analysis of IDR-1010cys in Free Form and Its Soluble Conjugate in the Presence of Lipid SUVs

Structural content of IDR-1010cys and polymerC-1010cys, as a function of (A) IDR-1010cys-to-DPC ratios of 1:15, 1:50, and 1:100; (B) IDR-1010cys-to-DMPC/DMPG ratios of 1:15, 1:50, and 1:100; (C) polymerC-1010cys-to-DPC ratios of 1:15, 1:50, and 1:100; and (D) polymerC-1010cys-to-DMPC/DMPG ratios of 1:15, 1:50, and 1:100. The structural content was determined using the CD-fitting programs CDSSTR, SELCON3, and CONTINLL, applied to the data shown in Figure 3.

Some interesting observations were noted in the case of surface-tethered peptides. The polymer brush acts as a flexible linker between the peptide and the surface. Although significantly larger amounts of peptide per unit area can be conjugated to a surface via polymer brush compared to the direct grafting of peptides (Gao et al., 2011a, 2011b; Barbey et al., 2009; Ayres, 2010), the polymer brush structure could potentially exert steric restrictions. This may hinder the interaction of the peptides with biomembranes. The data presented here suggest that in the presence of lipid SUVs, there was no quantitative change in the helical content of the surface-tethered peptides, unlike the case of free peptides; the presence of unstructured peptides was evident. One plausible reason might be the fact that the peptides that were buried deep into the brush layer were not sterically capable of interacting with the lipid SUVs.

Interestingly, the surface-tethered peptides adopted more helical structure in comparison to soluble polymer-conjugated peptides (quartz-brush-1010cys versus polymerC-1010cys; Figures 4 and 5B). Because there were more (ca. 300) peptides attached per chain of polymerC-1010cys compared to quartz-brush-1010cys (ca. 50–100 peptides/chain), peptide-peptide interactions could not account for the higher α-helical content observed in the case of surface-tethered peptides. The fact that the peptides were less structured in the case of polymerC-1010cys than in the case of surface-tethered peptides suggests that the peptides might be less exposed to the SUVs. This finding is surprising if one considers that the SUVs may be restricted from diffusing into the peptide/polymer brushes packed together on a surface. Our soluble polymer data suggest that the peptides can self-assemble due to the conformational freedom of linear chains, as reported in the case of other systems (ten Cate and Börner, 2007; Paira et al., 2010; Verch et al., 2010). This self-assembly would restrict the interactions of the peptides with lipid SUVs. Our data also show that the current soluble copolymer structure, at least in the present form and with the current peptide, may not be an ideal scaffold for enhanced membrane interaction.

Although polymerC-1010cys and quartz-brush-1010cys have similar compositions, the attached peptides behaved differently in terms of their interaction with lipid SUVs in these cases: the surface-tethered peptide interacted more favorably with lipid SUVs. The observed differences can be attributed to the following facts. It is possible that the distribution of peptides attached to the polymer chains within the surface-grafted brush is playing a role in the observed differences. In the case of the polymer brush system, there may be a higher density of peptides near the outer surface of the brushes. This is attributable to the restricted diffusion of large molecules within the brush layer (Steels et al., 2000). This higher local concentration of peptides may translate into a higher relative number of peptides being exposed to the lipids, thereby resulting in higher helical content. It is important to note that because there are no data currently available on the distribution of peptides within polymer brush layers, it is difficult to exactly predict the influence of this parameter on structure and membrane interaction.

From our results, it is clear that the peptides in quartz-brush-1010cys can adopt different secondary structures under different conditions (Figure 5). Unlike the cases of peptide in the free form or conjugated to a soluble polymer (Figures 3 and 4), the surface-tethered IDR-1010cys has more structured components in water and PBS solution (Figures 3A, 3D, and 5Aa). Even in the dry state, the polymer brush-tethered peptide has more structured components that did not change significantly with hydration. The presence of structured peptide components in the case of quartz-brush-1010cys might be due to the interaction of the peptide with the hydrophobic components of the grafted polymer chains. Even though the copolymer is highly soluble in water, it is composed of a hydrophobic backbone consisting of repeating (-CH_2-CH_2-) groups and a hydrophobic propyl group as side chain (from APMA). In other words, the hydrophobic nature of the polymer may favor interactions that are similar to those found between the peptide and lipid membrane. It is interesting to note that the higher structural content was found for the peptides tethered to polymers that contained higher amounts of DMA as compared to APMA (Figure 5Bc). The higher APMA content allows the peptide to graft more closely. Thus, the brush composition has imposed an

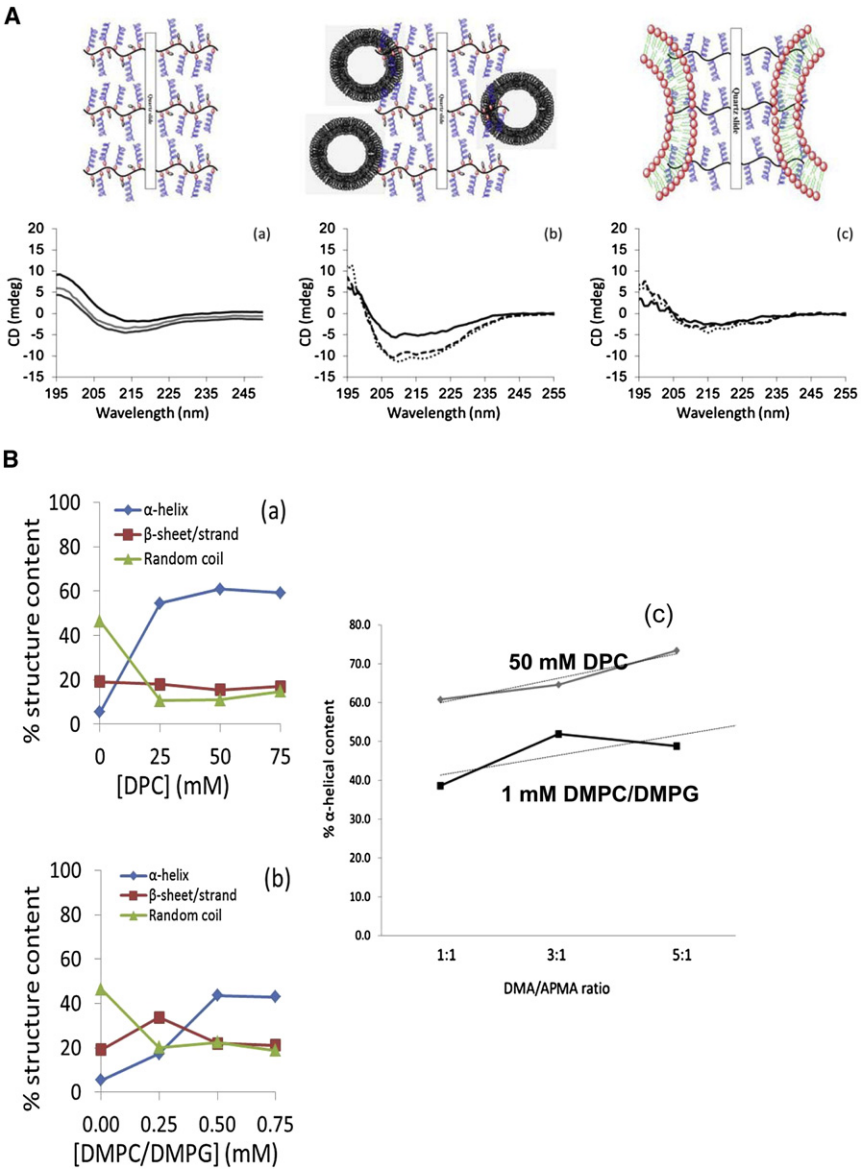

Figure 5. Biomembrane Interactions of Surface-Immobilized IDR-1010cys

(A) CD spectra of quartz-brush-1010cys: (a) in the absence of solvent (top), in H_2O (middle), and in PBS (bottom); (b) in the presence of DPC; and (c) in the presence of DMPC:DMPG (1:1). In (b), the concentration of DPC was 25 mM (solid), 50 mM (dashed), and 75 mM (dotted). In (c), the concentration of DMPC/DMPG was 0.25 mM (solid), 0.50 mM (dashed), and 0.75 mM (dotted). The data are shown for the brush chemical composition of 1:1 DMA:APMA (w/w).

(B) Structural content of quartz-brush-1010cys, as a function of (a) DPC concentration, (b) DMPC/DMPG concentration, and (c) DMA:APMA ratio in 50 mM DPC (gray) and 1 mM DMPC/DMPG (black). The dashed lines are trend lines. The structural content was determined using the CD-fitting programs CDSSTR, SELCON3, and CONTINLL, applied to the data shown (A). A brush chemical composition of 1:1 DMA:APMA (w/w) was used for plots (a) and (b).

important effect on the polymer-peptide, peptide-peptide, and peptide-lipid SUV interactions.

The peptide conformation in the brush layer was also found to be dependent on lipid concentration. As the DPC concentration increased, so did the α-helical content. A similar trend was observed for the peptide exposed to 1:1 DMPC:DMPG (mol/mol) SUVs. In order to understand the significance of these observations and relate them back to what happens for the free peptide, it is important to compare the relative concentrations of peptide and lipid used under different conditions. With the surface area of the slide covered in brushes being 685 mm^2 and the number of peptides/area for the 1:1 DMA:APMA sample being 7.5 peptides/nm^2, there was a total of ~5,150 peptides or 8.6 × 10^{-21} mol of peptide in quartz-brush-1010cys. The lipid concentrations range from 0.25 to 75 mM. In the case of free peptide, the amount of peptide was 1 × 10^{-7} mol, with the lipid concentration ranging between 3 and 20 mM. In other words, the total concentration of the peptide was minute in the tethered samples. Comparing the helical content observed for the free peptide (~99%–60%) to the helical content observed for quartz-brush-1010cys (1:1 DMA:APMA) (~60%) in the presence of lipid suggested that proportionately more peptides were structured in the tethered case than when the peptide was in free form. As discussed above, the distribution of peptides found in the tethered samples might result in higher local concentrations of peptides (Table 1), which in turn could translate into a higher relative number of peptides being exposed to the lipids, thereby resulting in higher helical content per mole of peptide.

Based on the results, we propose a model for the possible mechanism of action of polymer brush-immobilized peptide IDR-1010cys (Figure 6): (1) the peptide tethered to the polymer brush adopts some structure due to interactions with the polymer chains; (2) when exposed to lipids, more of the peptides adopt structure; and (3) as the local concentration of peptide tethered to the brush is high, the amount of membrane insertion or disruption of membrane electrostatics is high and consequently the damage to the membrane permeability barrier is large. This is in contrast to the free peptide, where membrane interaction and perturbation are diffusion limited. It is important to note that the proposed mechanism shown in Figure 6 assumes that IDR-1010cys functions by perturbing bacterial membranes. If the mode of action involves targets other than the membrane, then perhaps the high local concentration is a key factor in the differences observed.

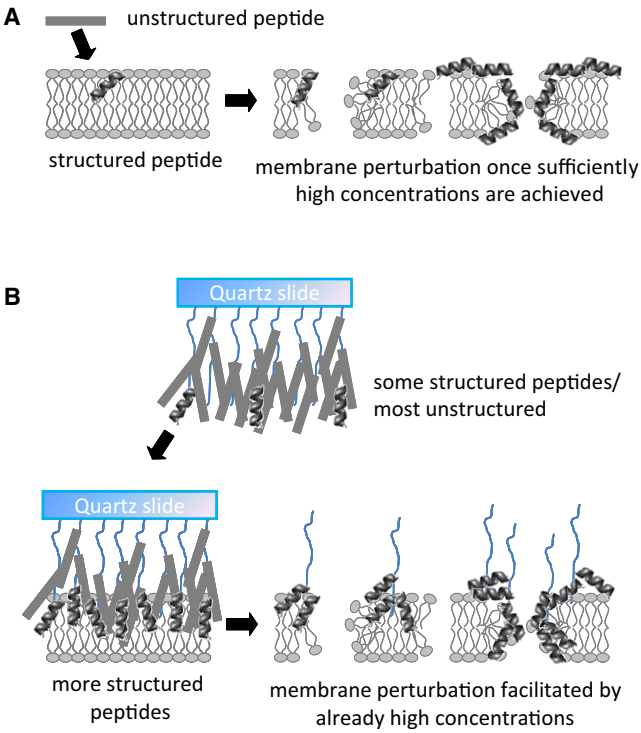

Figure 6. Proposed Mechanism of Action
Free peptide (A) and polymer brush-immobilized host defense peptide (B) are shown. Note that only half the quartz slide is illustrated for purposes of clarity. In (B), more peptides adopt a structure before they interact with the membrane, and therefore there are perhaps more structured peptides localized in one area when they bind/insert into the membrane. As a result, perturbation of the membrane may be more efficient.

SIGNIFICANCE

Detailed understanding of the mechanism of action of surface-tethered antimicrobial and immunomodulatory peptides is very important in the design of highly efficient antimicrobial and antibiofilm coatings. The data presented here suggest that tethered peptides interact with lipid SUVs differently from free peptide or peptide tethered to a soluble polymer, perhaps due to the high local concentration. It has been postulated that the disturbance of surface electrostatics at the bacterial surface upon interaction with tethered peptides may trigger an autolytic and/or cell death mechanism (Jelokhani-Niaraki et al., 2002; Resende et al., 2009). Our results with quartz-brush-1010cys also point to such a mechanism of action. The high local charge density associated with the peptide tethering at the surface, the flexibility of the polymer brush linker, and conformational restrictions of polymer chains within the brush (unlike the case of soluble copolymer chains) all contribute to the enhanced interaction of the peptide with the model lipid membranes. Although the soluble copolymer and the polymer brush structure have similar compositions, the polymer brush-conjugated peptide was much more structured and would therefore be expected to be a more effective bactericidal agent than peptide attached to soluble supports. Interestingly, the interactions of the surface-tethered and soluble polymer-conjugated IDR-1010cys with lipid SUVs are well correlated with their antimicrobial and immunomodulatory activities. PolymerC-1010cys showed less biological activity as well as membrane interaction compared to surface-tethered IDR-1010cys. Thus, the optimization of surface density of peptides and linker chemistry is critical to the development of highly effective antimicrobial coatings.

EXPERIMENTAL PROCEDURES

Details of materials and methods are given in Supplemental Experimental Procedures.

Synthesis of Copolymer Brushes

Initiator Modification

Quartz slides (38.1 × 9.0 × 1.0 mm), cut from quartz microscopy slides (38.1 × 25.4 × 1.0 mm; Alfa Aesar), were treated with piranha solution at 70°C for 4 hr. The slides were washed with distilled water and dried in a stream of argon. The primary amine-modified quartz slides were obtained by refluxing in a 1 wt% 3-aminopropyltrimethoxysilane in toluene solution. After 2 hr, the slides were ultrasonicated consecutively with toluene, acetone, dichloromethane, and dried in a stream of argon.

Amine-modified quartz surface was treated with 2-chloropropionyl chloride (2.50 g, 19.68 mmol) and triethylamine (2.17 g, 21.40 mmol) in dichloromethane (30 ml) at 0°C over a period of 2 hr. The reaction was continued at 0°C for 4 hr and left overnight at room temperature. The modified surfaces were cleaned by ultrasonication in dichloromethane, acetone, methanol, and water consecutively, and preserved in argon after drying in vacuum.

Surface-Initiated Atom Transfer Radical Polymerization of DMA and APMA

All the polymerization experiments were conducted in a glove box filled with argon. For a typical experiment, DMA (0.5 g, 5 mmol) and APMA (0.9 g, 5 mmol) were dissolved in degassed purified water (4.5 ml). This solution was introduced into a mixture of $CuCl_2$ (0.5 mg, 3.7×10^{-3} mmol), CuCl (3.7 mg, 3.7×10^{-2} mmol), and HMTETA (1,1,4,7,10,10-hexamethyltriethylenetetramine; 22 μl, 8.1×10^{-2} mmol), and then stirred until homogeneous. A quartz slide modified with atom transfer radical polymerization (ATRP) initiator was introduced to the polymerization mixture along with the addition of methyl-2-chloropropionate (4.3 μl [in 10% ethanol solution], 3.7×10^{-3} mmol) and the polymerization was continued at 22°C for 24 hr. The polymerization was stopped by exposing it to air and followed by dilution with water. The resulting copolymer-grafted quartz slide was ultrasonicated in water twice (15 min each) and dried in vacuum. The solution polymer formed along with the surface-grafted polymer was dialyzed against water for 2 days (MWCO 1,000 membranes) and the polymer was obtained by lyophilization.

The initial comonomer ratio (DMA:APMA) was varied from 5:1 to 3:1 to 1:1 to obtain copolymer brushes with different amine content. Dry thickness of the polymer film on the quartz surface was measured by atomic force microscopy scratch analysis. The graft densities were calculated using the following equation (Wu et al., 2003; Zou et al., 2009):

$$\sigma = \frac{h \times \rho \times N_A}{M_n}, \qquad \text{(Equation 1)}$$

where σ is graft density, M_n is the number average molecular weight of grafted chains, h is polymer film thickness, ρ is density of copolymer (1.20 g/ml), and N_A is Avogadro's number.

Peptide Conjugation to Polymer Brush

Maleimide Group Conjugation. The copolymer brush on the quartz slide was initially incubated with an aqueous solution of 0.5 M Et_3N (20 ml) for 20 min. The surface was then washed with water and ultrasonicated consecutively with water, acetone, and methanol, and dried. The surface was then treated with 3-maleimidopropionic acid *N*-hydroxysuccinimide (1 M solution, 4 ml) in acetonitrile for 6 hr at 22°C, ultrasonicated consecutively in acetonitrile and acetone, and dried in argon flow.

Peptide IDR-1010cys Conjugation. The maleimide-modified quartz slides from the previous step were treated with a solution of cysteine containing

peptide IDR-1010cys (IRWRIRVWVRRIC) (10 ml of a 1 mg/ml solution) in 0.1 M sodium phosphate buffer overnight followed by an excess of 2-mercaptoethanol (0.1 g/ml) for another day. The peptide-immobilized quartz slide was cleaned ultrasonically with water twice (15 min each) and the samples were dried in argon flow. The dried samples were stored under argon and characterized by UV-vis and AFM analysis. UV-vis spectra (Varian Cary 4000 spectrophotometer) of IDR-1010cys-immobilized quartz slides were collected after inserting the peptide-conjugated quartz slide (38.1 × 9.0 × 1.0 mm) into a 1 cm quartz cell. The number of peptides/chain was calculated from the polymer film thickness increase after IDR-1010cys conjugation, amount of polymer grafted, molecular weight, and graft density (see Supplemental Information for details).

Synthesis of Peptide IDR-1010cys-Conjugated Soluble Copolymer; PolymerC-1010cys

Poly(DMA-*co*-APMA) (0.2 g) (DMA:APMA molar ratio 1:1, M_n 1.66 × 10^5, M_w:M_n 1.18; sample Q-1-1 in Table 1), formed along with surface-grafted copolymer chains, was dissolved in water (5 ml) and added to Et_3N (0.5 ml). After stirring for 2 hr at room temperature, the polymer was precipitated in acetone and dried in vacuum. The purified polymer (0.12 g) was dissolved in acetonitrile (5 ml) and added to 3-maleimidopropionic acid *N*-hydroxysuccinimide in acetonitrile solution (1 M solution, 5 ml) and stirred for 1 hr at 22°C. The maleimide-conjugated copolymer (0.08 g) was purified by precipitating in EtOAc two times and dried in vacuum. The modified polymer was characterized by NMR.

The maleimide-conjugated polymer (8 mg) was dissolved in 1 ml sodium phosphate buffer and added to a cysteine-containing peptide IDR-1010cys solution (2 ml of an 8 mg/ml solution) in sodium phosphate buffer and stirred overnight at room temperature. The IDR-1010cys-conjugated polymer (10.25 mg) was recovered by lyophilization after dialysis against water for 4 days. The conjugate was characterized by NMR and UV-vis analyses (Figure S3).

Antimicrobial Activity of Peptide IDR-1010 and Copolymer Conjugate

Antimicrobial activity was measured as described previously (Wieczorek et al., 2010), assessing both MIC and rate of killing in Mueller Hinton medium.

Immunomodulatory Activity of Peptide IDR-1010

Venous blood from healthy volunteers was collected in Vacutainer collection tubes containing sodium heparin as an anticoagulant (BD Biosciences) in accordance with University of British Columbia ethical approval and guidelines. Isolation of PBMCs and cell stimulations were performed as described previously (Nijnik et al., 2010). Following 24 hr of exposure to the peptide samples, the tissue culture supernatants were centrifuged at 16,000 × g (13,000 rpm) at 4°C for 5 min in an IEC MicroMax centrifuge to obtain cell-free samples. Supernatants were aliquoted and then stored at –20°C before assay for monocyte chemoattractant protein 1. MCP-1 secretion in the tissue culture supernatants was detected by sandwich ELISA kits (eBioscience). All assays were performed in triplicate. The concentration of chemokines in the culture medium was quantified by establishing a standard curve with serial dilutions of the recombinant human MCP-1. Secretion of TNF-α was monitored in rested PBMCs, and cells were exposed to peptide and/or LPS by capture ELISA after 24 hr (eBioscience).

All mouse experiments were conducted in accordance with the Animal Care Ethics Approval and Guidelines of the University of British Columbia. C57BL/6J mice (The Jackson Laboratory) were maintained under specific pathogen-free conditions. Animal models of progressive *S. aureus* infection were performed as described previously (Nijnik et al., 2010).

Circular Dichroism Spectroscopy Analysis

CD spectroscopy analysis of surface-immobilized IDR-1010cys was performed using a Jasco J-800 spectropolarimeter and 1 cm path length quartz cell for quartz surface samples and 0.2 cm path length quartz cell for solution samples. The data were acquired after inserting the peptide-conjugated quartz slide (38.1 × 9.0 × 1.0 mm) into a 1 cm quartz cell (see Figure S4). A copolymer brush-conjugated quartz slide was used as a control sample.

For solution CD experiments, solutions were prepared at a constant peptide concentration of 0.2 mM (peptide alone or poly(DMA-*co*-APMA) copolymer conjugated) at different P:L molar ratios, using lipid mixtures of DMPC:DMPG (1:1 molar ratio) or DPC. Appropriate amounts of lipids in chloroform were dried using a stream of nitrogen gas to remove most of the chloroform and vacuum dried overnight in a 5 ml round bottom flask. After adding 450 μl of PBS and 0.1 μmol of peptide in PBS (50 μl) to the dried lipids, the mixture was sonicated in a water bath for a minimum of 30 min (until the solution was no longer turbid) to ensure lipid vesicle formation. For all samples, corresponding background samples without peptides were prepared for spectral subtraction.

CD analysis of surface-immobilized peptide samples was performed in a similar fashion. Dry lipids were dissolved in chloroform and dried overnight in a 5 ml round bottom flask. PBS solutions of the lipids (DPC or DMPC:DMPG [1:1 molar ratio] mixture) were prepared at different concentrations and sonicated in a water bath for approximately 30 min (until the solution was no longer turbid). Then the lipid solution was pipetted into the quartz cell. Corresponding background samples were run initially without placing the sample quartz slide in the quartz cell.

Solution and surface CD experiments were carried out at 30°C. The temperature of the sample compartment was kept constant by means of a water bath. The spectra were obtained over a wavelength range of 190–250 nm, using continuous scanning mode with a response of 1 s with 0.5 nm steps, a bandwidth of 1.5 nm, and a scan speed of 50 nm/min. The signal:noise ratio was increased by acquiring each spectrum over an average of three scans. Finally, each spectrum was corrected by subtracting the background from the sample spectrum.

To examine the extent of secondary structure content of IDR-1010cys and surface-tethered IDR-1010cys in different environments, all spectra were fitted using three different programs (CDSSTR, CONTINLL, and SELCON3), as described elsewhere (Cheng et al., 2010, 2011).

SUPPLEMENTAL INFORMATION

Supplemental Information includes one table, five figures, and Supplemental Experimental Procedures and can be found with this article online at doi:10.1016/j.chembiol.2011.12.015.

ACKNOWLEDGMENTS

This research was supported by the Natural Science and Engineering Council of Canada and by the Canadian Institutes of Health Research (CIHR) through a Collaborative Health Research Projects grant. J.N.K. acknowledges a New Investigator award from CIHR and the Canadian Blood Services, and the Michael Smith Foundation for Health Research (MSFHR) Career Scholar Award. R.E.W.H. holds a Canada Research Chair. J.K. held a postdoctoral fellowship from the Canadian Cystic Fibrosis Foundation during this work. S.K.S. acknowledges funding from MSFHR in the form of a Career Scholar Award. The authors thank the Laboratory of Molecular Biophysics Macromolecular Hub and Spectroscopy Hub at the UBC Centre for Blood Research for the use of their research facilities, which is supported by the Canadian Foundation for Innovation and the MSFHR.

Received: August 11, 2011
Revised: November 30, 2011
Accepted: December 16, 2011
Published: February 23, 2012

REFERENCES

Ayres, N. (2010). Polymer brushes: applications in biomaterials and nanotechnology. Polym. Chem. *1*, 769–777.

Bagheri, M., Beyermann, M., and Dathe, M. (2009). Immobilization reduces the activity of surface-bound cationic antimicrobial peptides with no influence upon the activity spectrum. Antimicrob. Agents Chemother. *53*, 1132–1141.

Barbey, R., Lavanant, L., Paripovic, D., Schüwer, N., Sugnaux, C., Tugulu, S., and Klok, H.A. (2009). Polymer brushes via surface-initiated controlled radical polymerization: synthesis, characterization, properties, and applications. Chem. Rev. *109*, 5437–5527.

Blin, T., Purohit, V., Leprince, J., Jouenne, T., and Glinel, K. (2011). Bactericidal microparticles decorated by an antimicrobial peptide for the easy disinfection of sensitive aqueous solutions. Biomacromolecules *12*, 1259–1264.

Bowdish, D.M., Davidson, D.J., Scott, M.G., and Hancock, R.E. (2005). Immunomodulatory activities of small host defense peptides. Antimicrob. Agents Chemother. *49*, 1727–1732.

Cheng, J.T., Hale, J.D., Kindrachuk, J., Jenssen, H., Elliott, M., Hancock, R.E., and Straus, S.K. (2010). Importance of residue 13 and the C-terminus for the structure and activity of the antimicrobial peptide aurein 2.2. Biophys. J. *99*, 2926–2935.

Cheng, J.T., Hale, J.D., Elliott, M., Hancock, R.E., and Straus, S.K. (2011). The importance of bacterial membrane composition in the structure and function of aurein 2.2 and selected variants. Biochim. Biophys. Acta *1808*, 622–633.

Costerton, J.W., Stewart, P.S., and Greenberg, E.P. (1999). Bacterial biofilms: a common cause of persistent infections. Science *284*, 1318–1322.

Darouiche, R.O. (2001). Device-associated infections: a macroproblem that starts with microadherence. Clin. Infect. Dis. *33*, 1567–1572.

Darouiche, R.O. (2004). Treatment of infections associated with surgical implants. N. Engl. J. Med. *350*, 1422–1429.

Foxman, B. (2002). Epidemiology of urinary tract infections: incidence, morbidity, and economic costs. Am. J. Med. *113* (*Suppl 1A*), 5S–13S.

Gao, G., Lange, D., Hilpert, K., Kindrachuk, J., Zou, Y., Cheng, J.T., Kazemzadeh-Narbat, M., Yu, K., Wang, R., Straus, S.K., et al. (2011a). The biocompatibility and biofilm resistance of implant coatings based on hydrophilic polymer brushes conjugated with antimicrobial peptides. Biomaterials *32*, 3899–3909.

Gao, G., Yu, K., Kindrachuk, J., Brooks, D.E., Hancock, R.E.W., and Kizhakkedathu, J.N. (2011b). Antibacterial surfaces based on polymer brushes: investigation on the influence of brush properties on antimicrobial peptide immobilization and antimicrobial activity. Biomacromolecules *12*, 3715–3727.

Glinel, K., Jonas, A.M., Jouenne, T., Leprince, J., Galas, L., and Huck, W.T. (2009). Antibacterial and antifouling polymer brushes incorporating antimicrobial peptide. Bioconjug. Chem. *20*, 71–77.

Gollwitzer, H., Ibrahim, K., Meyer, H., Mittelmeier, W., Busch, R., and Stemberger, A. (2003). Antibacterial poly(D,L-lactic acid) coating of medical implants using a biodegradable drug delivery technology. J. Antimicrob. Chemother. *51*, 585–591.

Gottler, L.M., and Ramamoorthy, A. (2009). Structure, membrane orientation, mechanism, and function of pexiganan—a highly potent antimicrobial peptide designed from magainin. Biochim. Biophys. Acta *1788*, 1680–1686.

Goux, W.J. (2002). The conformations of filamentous and soluble tau associated with Alzheimer paired helical filaments. Biochemistry *41*, 13798–13806.

Hetrick, E.M., and Schoenfisch, M.H. (2006). Reducing implant-related infections: active release strategies. Chem. Soc. Rev. *35*, 780–789.

Hilpert, K., Volkmer-Engert, R., Walter, T., and Hancock, R.E. (2005). High-throughput generation of small antibacterial peptides with improved activity. Nat. Biotechnol. *23*, 1008–1012.

Hilpert, K., Elliott, M., Jenssen, H., Kindrachuk, J., Fjell, C.D., Körner, J., Winkler, D.F., Weaver, L.L., Henklein, P., Ulrich, A.S., et al. (2009). Screening and characterization of surface-tethered cationic peptides for antimicrobial activity. Chem. Biol. *16*, 58–69.

Husseman, M., Malmström, E.E., McNamara, M., Mate, M., Mecerreyes, D., Benoit, D.G., Hedrick, J.L., Mansky, P., Huang, E., Russell, T.P., et al. (1999). Controlled synthesis of polymer brushes by "living" free radical polymerization techniques. Macromolecules *32*, 1424–1431.

Iwata, R., Satoh, R., Iwasaki, Y., and Akiyoshi, K. (2008). Covalent immobilization of antibody fragments on well-defined polymer brushes via site-directed method. Colloids Surf. B Biointerfaces *62*, 288–298.

Jelokhani-Niaraki, M., Prenner, E.J., Kay, C.M., McElhaney, R.N., and Hodges, R.S. (2002). Conformation and interaction of the cyclic cationic antimicrobial peptides in lipid bilayers. J. Pept. Res. *60*, 23–36.

Kindrachuk, J., Jenssen, H., Elliott, M., Townsend, R., Nijnik, A., Lee, S.F., Gerdts, V., Babiuk, L.A., Halperin, S.A., and Hancock, R.E. (2009). A novel vaccine adjuvant comprised of a synthetic innate defence regulator peptide and CpG oligonucleotide links innate and adaptive immunity. Vaccine *27*, 4662–4671.

Kizhakkedathu, J.N., and Brooks, D.E. (2003). Synthesis of poly(*N*,*N*-dimethylacrylamide) brushes from charged polymeric surfaces by aqueous ATRP: effect of surface initiator concentration. Macromolecules *36*, 591–598.

Matl, F.D., Obermeier, A., Repmann, S., Friess, W., Stemberger, A., and Kuehn, K.D. (2008). New anti-infective coatings of medical implants. Antimicrob. Agents Chemother. *52*, 1957–1963.

Mookherjee, N., Wilson, H.L., Doria, S., Popowych, Y., Falsafi, R., Yu, J.J., Li, Y., Veatch, S., Roche, F.M., Brown, K.L., et al. (2006). Bovine and human cathelicidin cationic host defense peptides similarly suppress transcriptional responses to bacterial lipopolysaccharide. J. Leukoc. Biol. *80*, 1563–1574.

Nijnik, A., Madera, L., Ma, S., Waldbrook, M., Elliott, M.R., Easton, D.M., Mayer, M.L., Mullaly, S.C., Kindrachuk, J., Jenssen, H., and Hancock, R.E. (2010). Synthetic cationic peptide IDR-1002 provides protection against bacterial infections through chemokine induction and enhanced leukocyte recruitment. J. Immunol. *184*, 2539–2550.

Noimark, S., Dunnill, C.W., Wilson, M., and Parkin, I.P. (2009). The role of surfaces in catheter-associated infections. Chem. Soc. Rev. *38*, 3435–3448.

Onaizi, S.A., and Leong, S.S. (2011). Tethering antimicrobial peptides: current status and potential challenges. Biotechnol. Adv. *29*, 67–74.

Paira, T.K., Banerjee, S., Raula, M., Kotal, A., Si, S., and Mandal, T.K. (2010). Peptide-polymer bioconjugates via atom transfer radical polymerization and their solution aggregation into hybrid micro/nanospheres for dye uptake. Macromolecules *43*, 4050–4061.

Palermo, E.F., Lee, D.K., Ramamoorthy, A., and Kuroda, K. (2011). Role of cationic group structure in membrane binding and disruption by amphiphilic copolymers. J. Phys. Chem. B *115*, 366–375.

Ramstedt, M., Ekstrand-Hammarström, B., Shchukarev, A.V., Bucht, A., Osterlund, L., Welch, M., and Huck, W.T. (2009). Bacterial and mammalian cell response to poly(3-sulfopropyl methacrylate) brushes loaded with silver halide salts. Biomaterials *30*, 1524–1531.

Resende, J.M., Moraes, C.M., Munhoz, V.H., Aisenbrey, C., Verly, R.M., Bertani, P., Cesar, A., Piló-Veloso, D., and Bechinger, B. (2009). Membrane structure and conformational changes of the antibiotic heterodimeric peptide distinctin by solid-state NMR spectroscopy. Proc. Natl. Acad. Sci. USA *106*, 16639–16644.

Sambhy, V., MacBride, M.M., Peterson, B.R., and Sen, A. (2006). Silver bromide nanoparticle/polymer composites: dual action tunable antimicrobial materials. J. Am. Chem. Soc. *128*, 9798–9808.

Scott, M.G., Dullaghan, E., Mookherjee, N., Glavas, N., Waldbrook, M., Thompson, A., Wang, A., Lee, K., Doria, S., Hamill, P., et al. (2007). An anti-infective peptide that selectively modulates the innate immune response. Nat. Biotechnol. *25*, 465–472.

Shukla, A., Fleming, K.E., Chuang, H.F., Chau, T.M., Loose, C.R., Stephanopoulos, G.N., and Hammond, P.T. (2010). Controlling the release of peptide antimicrobial agents from surfaces. Biomaterials *31*, 2348–2357.

Sreerama, N., Venyaminov, S.Y., and Woody, R.W. (2000). Estimation of protein secondary structure from circular dichroism spectra: inclusion of denatured proteins with native proteins in the analysis. Anal. Biochem. *287*, 243–251.

Sreerama, N., Venyaminov, S.Y., and Woody, R.W. (2001). Analysis of protein circular dichroism spectra based on the tertiary structure classification. Anal. Biochem. *299*, 271–274.

Steels, B.M., Koska, J., and Haynes, C.A. (2000). Analysis of brush-particle interactions using self-consistent-field theory. J. Chromatogr. B Biomed. Sci. Appl. *743*, 41–56.

Straus, S.K., and Hancock, R.E. (2006). Mode of action of the new antibiotic for Gram-positive pathogens daptomycin: comparison with cationic antimicrobial peptides and lipopeptides. Biochim. Biophys. Acta *1758*, 1215–1223.

ten Cate, M.G.J., and Börner, H.G. (2007). Synthesis of ABC-triblock peptide-polymer conjugates for the positioning of peptide segments within block copolymer aggregates. Macromol. Chem. Phys. *208*, 1437–1446.

Trampuz, A., and Widmer, A.F. (2006). Infections associated with orthopedic implants. Curr. Opin. Infect. Dis. *19*, 349–356.

Verch, A., Hahn, H., Krause, E., Cölfen, H., and Börner, H.G. (2010). A modular approach towards functional decoration of peptide-polymer nanotapes. Chem. Commun. (Camb.) *46*, 8938–8940.

Wieczorek, M., Jenssen, H., Kindrachuk, J., Scott, W.R., Elliott, M., Hilpert, K., Cheng, J.T., Hancock, R.E., and Straus, S.K. (2010). Structural studies of a peptide with immune modulating and direct antimicrobial activity. Chem. Biol. *17*, 970–980.

Wu, T., Efimenko, K., Vlček, P., Šubr, V., and Genzer, J. (2003). Formation and properties of anchored polymers with a gradual variation of grafting densities on flat substrates. Macromolecules *36*, 2448–2453.

Zimmerli, W., Trampuz, A., and Ochsner, P.E. (2004). Prosthetic-joint infections. N. Engl. J. Med. *351*, 1645–1654.

Zou, Y., Rossi, N.A.A., Kizhakkedathu, J.N., and Brooks, D.E. (2009). Barrier capacity of hydrophilic polymer brushes to prevent hydrophobic interactions: effect of graft density and hydrophilicity. Macromolecules *42*, 4817–4828.